The effect of replacing molybdenum with vanadium on the tendency to amorphisation, structure and thermal properties of high-entropy alloys of the Fe–Co–Ni–Cr–(Mo,V)–B system

A. I. Bazlov · I. V. Strochko · E. N. Zanaeva · E. V. Ubyivovk · M. S. Parkhomenko · D. A. Milkova · V. V. Briukhanova

Received: 16 March 2023 / Revised: 1 May 2023 / Accepted: 15 September 2023

Abstract
This paper is dedicated to studying the effect of replacing molybdenum with vanadium on the tendency to amorphisation, structure, and thermal properties of high-entropy alloys of the $(Fe_{0.25}Ni_{0.25}Co_{0.25}Cr_{0.125}Mo_{0.125-x}V_x)_{100-y}B_y$ system, where $x = 0$; 0.0625; 0.125 and $y = 17–25$. The alloy structure was analyzed using X-ray diffraction, scanning and transmission electron microscopy methods. Thermal properties were determined by differential scanning calorimetry. It was found that the replacement of molybdenum with vanadium leads to the formation of crystalline particles of complex nitrides (V, Cr, Mo)(N, B) in the ribbon structure. The dependences of the characteristic alloy temperatures have been established. Molybdenum replacement with vanadium was shown to stabilize the supercooled liquid in alloys with completely amorphous structure.

Keywords Amorphous alloys · High-entropy alloys · Microstructure · Crystallization

Introduction

High-entropy alloys (HEAs), also referred to as multicomponent equiatomic alloys, were first synthesized in the early 2000s [1, 2] and immediately garnered significant scientific interest. Initially, HEAs were defined as alloys containing five or more components in equal atomic ratios. However, recent studies have shown that these alloys can contain elements in ratios close to equiatomic (e.g., ranging from 5 to 35%). High-entropy alloys exhibit high values of strength, hardness, wear resistance, as well as increased thermal stability, which creates a solid potential for their commercial applications [3–7]. The structure of high-entropy alloys typically consists of either FCC or BCC solid solutions or a mixture thereof, which is attributed to the high entropy value of alloy mixing [8, 9]. To predict the possibility of achieving a single-phase state, criteria related to interactions between the atomic pairs within the alloy composition (e.g., S_{mix}, H_{mix}, δ) have been developed [8]. In addition to forming a single-phase structure, the high-entropy approach was used when synthesizing bulk metallic glasses (BMGs) [10–13]. In order to form BMGs, the alloys should meet the following three conditions (Inoue's criteria): 1) possess large negative enthalpy of component mixing; 2) contain at least three components; and 3) possess a large difference in atomic radii of the components (> 10%) [14]. The first two conditions are suitable for forming single-phase high-

Translated from *Metallurg*, No. 11, pp. 86–92, November, 2023. https://doi.org/10.52351/00260827_2023_11_86

difference in atomic radii is high (δ > 9), while in crystalline single-phase HEAs, it is low (δ < 7) [9]. By using a combined approach, amorphous ferromagnetic high-entropy alloys of the (FeCoNi)BSi system were obtained [15, 16]. It was shown that the addition of chromium increases corrosion resistance of the alloys and stabilizes the size of the solid solution nanocrystals during crystallization [17, 18]. Partial replacement of chromium with molybdenum leads to the formation of high-strength alloys of the Fe–Co–Ni–Cr–Mo–B system over a wide range of boron concentrations [19]. The effect of molybdenum on the mechanical properties of the (FeCoNiCrMo)B alloys with different boron concentrations is inconclusive. For instance, alloys containing 11 to 15% boron exhibit lower strength at higher boron contents, which is attributed to the formation of an amorphous phase with a larger interatomic distance [20]. Such behavior of high-entropy amorphous alloys is the opposite of what is observed in case of (Fe,Co)BSi and Fe–B alloys [17, 21], when an increase in boron content leads to a less dense amorphous atomic configuration. The expansion or contraction of the first coordination sphere is related to the presence of early transition metals in the composition.

Vanadium is also an early transition metal, and its atomic radius has an intermediate value between iron and molybdenum. Addition of vanadium to the alloy can significantly affect the size of the first coordination sphere, which in turn will affect the mechanical properties of the alloys. However, it was noted that vanadium is rarely added to amorphous and crystalline high-entropy alloys based on iron. There are only a few studies indicating a positive effect of vanadium addition on the alloy strength and thermal stability [22–24]. High-entropy amorphous alloys based on the Fe–Co–Ni–Cr–B system with additions of early transition metals have not been sufficiently studied. In addition, there is a lack of studies dedicated to analyzing the effect of vanadium doping on the alloy tendency to amorphisation. The *objective of this study* is to determine the effect of partial or complete replacement of molybdenum with vanadium in high-entropy alloys, such as $Fe_{0.25}Ni_{0.25}Co_{0.25}Cr_{0.125}Mo_{0.125-x}V_x)_{100-y}B_y$, where $x = 0$; 0.0625; 0.125 and $y = 17$–25, on the tendency to amorphisation, and to establish the dependence of the alloy structure and crystallization process on the boron content.

Materials and procedures

The alloys were produced via melting in an argon-arc furnace using a water-cooled copper crucible. Upon evacuation to $5 \cdot 10^{-3}$ Pa, the furnace chamber was filled with argon (purity—99.9995%) to a pressure of $7 \cdot 10^4$ Pa. The charge materials included pieces of metals (purity—at least 99.9%), preliminary alloy (Ni–50 wt. % Mo), and crystalline boron (purity—99.8%). To achieve a homogeneous composition across the ingot cross-section, five remelts were conducted while turning the ingot. The charge mass was measured with an accuracy of 0.05 g, and the difference in mass between the initial charge and the resulting ingot did not exceed 0.1 g, which corresponds to 0.5% [25, 26].

The nitrogen content of the studied alloys was determined by reduction melting in an inert gas flow. The nitrogen content of all alloys did not exceed 0.045 wt. %, which is the average value for alloys based on the Fe–Ni–Cr alloying system.

The obtained alloys were used to produce 25 to 30 µm thick ribbons by employing a melt-spinning technique, according to which the melt was quenched onto a rotating copper disc. Both melting and quenching processes were carried out in argon at $3 \cdot 10^4$ Pa after preliminary evacuation of the chamber to $7 \cdot 10^{-4}$ Pa. The linear rotation velocity of the disc was 42 m/s.

The X-ray diffraction (XRD) analysis of the obtained alloys was performed using a Bruker D8 Advance diffractometer. Imaging was conducted according to the Bragg-Brentano geometry, while using Cu K_α radiation and a reflected-beam monochromator. The microstructure of the ribbons was analyzed via scanning and transmission electron microscopy using Zeiss Merlin and Zeiss Libra 200 microscopes.

The characteristic temperatures of the alloys were determined by differential thermal analysis using a Labsys Setaram calorimeter. Heating and cooling were carried out at a rate of 0.67 K/s in Al_2O_3 crucibles in high-purity argon. The accuracy of measuring phase transformation temperature was 1 K.

Results and discussion

Alloys of the $(Fe_{0.25}Ni_{0.25}Co_{0.25}Cr_{0.125}Mo_{0.125-x}V_x)_{100-y}B_y$ system, where $x = 0$; 0.0625; 0.125 and $y = 17$–25, were obtained by quenching the melts onto a rotating copper disc (melt-spinning technique), followed by categorization into Mo–B, Mo,V–B, and V–B alloy groups. The chemical compositions of the studied alloys are shown in Table 1.

The XRD patterns of the resulting alloys are shown in Fig. 1. All studied alloys of the Mo–B group possess an amorphous structure. The XRD patterns exhibit a broad diffuse maximum and no sharp crystalline reflections, which is indicative of the formation of an amorphous phase during quenching. Partial replacement of molybdenum with vanadium leads to the formation of a composite structure upon quenching in alloys containing 17 and 20 at. % boron. The structure of these alloys consists of a mixture of an amorphous matrix and crystalline particles with an FCC lattice. Complete replacement of molybdenum with vanadium results in the formation of a similar two-phase structure in the V–B group alloys until the boron content reaches 22 at. %. The demonstrated effect of boron content on the formation of amorphous phase during quenching correlates well with a commonly

Table 1 Chemical composition of studied alloys

Group	Designation	Alloying element content, at. %						
		Fe	Ni	Co	Cr	Mo	V	B
Mo–B	Mo–17B	20.75	20.75	20.75	10.375	10.375	0	17
	Mo–20B	20.75	20.75	20.75	10.375	10.375	0	20
	Mo–22B	20.75	20.75	20.75	10.375	10.375	0	22
	Mo–25B	20.75	20.75	20.75	10.375	10.375	0	25
Mo,V–B	Mo,V–17B	20.75	20.75	20.75	10.375	5.1875	5.1875	17
	Mo,V–20B	20.75	20.75	20.75	10.375	5.1875	5.1875	20
	Mo,V–22B	20.75	20.75	20.75	10.375	5.1875	5.1875	22
	Mo,V–25B	20.75	20.75	20.75	10.375	5.1875	5.1875	25
V–B	V–17B	20.75	20.75	20.75	10.375	0	10.375	17
	V–20B	20.75	20.75	20.75	10.375	0	10.375	20
	V–22B	20.75	20.75	20.75	10.375	0	10.375	22
	V–25B	20.75	20.75	20.75	10.375	0	10.375	25

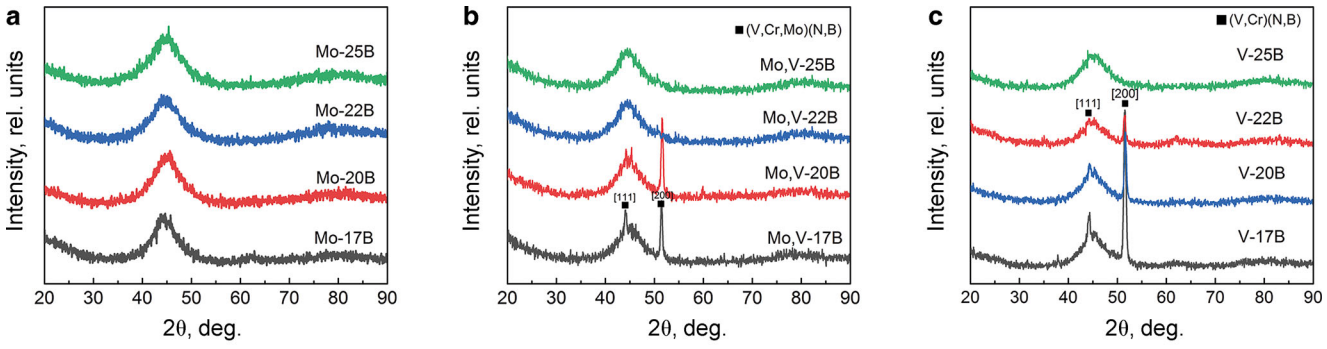

Fig. 1 Diffraction patterns of alloys: **a** Mo-B group; **b** Mo,V–B group; **c** V–B group

observed increase in the glass-forming ability of iron-based amorphous alloys at higher concentrations of boron [19, 27]. To determine the chemical composition of the crystallizing phases, microstructure studies and X-ray microanalysis of the alloys were conducted. SEM micrographs of the cross-sections of ribbons obtained from the studied alloys are shown in Fig. 2.

The microstructure of the Mo–20B alloy ribbon is homogeneous. There is no phase contrast, which confirms the formation of a uniform amorphous structure. Partial and complete replacement of molybdenum with vanadium leads to the formation of crystals in the ribbon structure, which protrude on the air-facing surface of the ribbon. The observed crystals have a faceted shape. It should be noted that the crystals are evenly distributed along the entire length of the ribbon, but only on the air-facing side of it.

The results of the X-ray microanalysis analysis of the studied alloys are shown in Table 2. Due to inaccuracies of determination, boron and nitrogen were excluded from the analytical results. It was found that boron is present both in the amorphous matrix and in the crystals, while an increased nitrogen content is only observed in crystals.

The ratio of alloying elements in the matrix is close to the nominal composition of the alloys. However, the compositions of crystals observed in the Mo,V–20B and V–20B alloys differ significantly from the matrix. These crystals represent particles of solid solutions of chromium and molybdenum in vanadium. It is important to note that all these elements form continuous series of solid solutions with a body-centered cubic (BCC) lattice [28–30]. At the same time, the X-ray diffraction patterns show a set of reflections that are characteristic of a face-centered cubic (FCC) lattice with a period of 0.356 nm. Such crystalline lattice is typical for vanadium and chromium compounds with nitrogen (e.g., VN, CrN), as well as complex nitrides of chromium and vanadium of variable compositions (e.g., (VCr)N). The increased content of boron and nitrogen suggests that the observed crystals are complex nitrides, such as (V,Cr,Mo)(N,B) and (V,Cr)(N,B). Although these crystals are based on vanadium, chromium, and molybdenum, they also contain a small amount of other dissolved metals. Nitrides with a stoichiometric metals to nitrogen ratio of 1:1 are characterized by a high melting temperature (in excess of 2000 °C), and are poorly soluble in the melt. The formation of boron-enriched nitrides leads to a reduction in its concentration in the amorphous matrix.

The structure of the V–22B alloy was studied using TEM (Fig. 3). The data resulting from the analysis of the microstructure and diffraction patterns obtained from different areas confirm the formation of an amorphous phase and crystals with a cubic lattice embedded therein (see Fig. 3b). A high-resolution TEM image of the crystal—amorphous matrix interface is shown in Fig. 3a. The diffraction pattern obtained from the amorphous phase area shows a diffuse halo (see Fig. 3c) without crystalline spikes, thus confirming the absence of nanocrystals in the structure.

In order to establish a qualitative distribution of alloying elements in the structural components, the section containing both amorphous and crystalline phases was subjected to element mapping using X-ray microanalysis. A high-angle annular dark-field (HAADF) image of the section containing both amorphous and crystalline phases is shown in Fig. 3d along with the chemical element distribution. It was confirmed that, in addition to chromium and vanadium, the crystalline phase is enriched with nitrogen and boron as compared to the amorphous matrix. It is known that boron is highly soluble in zirconium and hafnium nitrides [31], which have a similar structure to that of vanadium and chromium nitrides, whereas nitrogen is practically insoluble in vanadium and chromium borides [32].

To analyze the effect of replacing molybdenum with vanadium in (FeCoNiCrMoV)B alloys on the characteristic temperatures of the alloys, a DSC analysis was performed. The DSC curves of the studied alloys are shown in Fig. 4.

All studied alloys demonstrate a multistage crystallization process. The crystallization of all Mo–B group alloys begins from the amorphous state, with no supercooled liquid region observed on the DSC curves. As the boron content in the alloy composition increases, the nature of the first exothermic peak changes from broad to sharp, which is caused by a change in the crystallization mechanism in this type of alloys [17]. The replacement of molybdenum with vanadium leads to a change in the nature of crystallization. For example, in alloys containing from 17 to 22 at. % boron, a separate exothermic peak is observed, corresponding to the

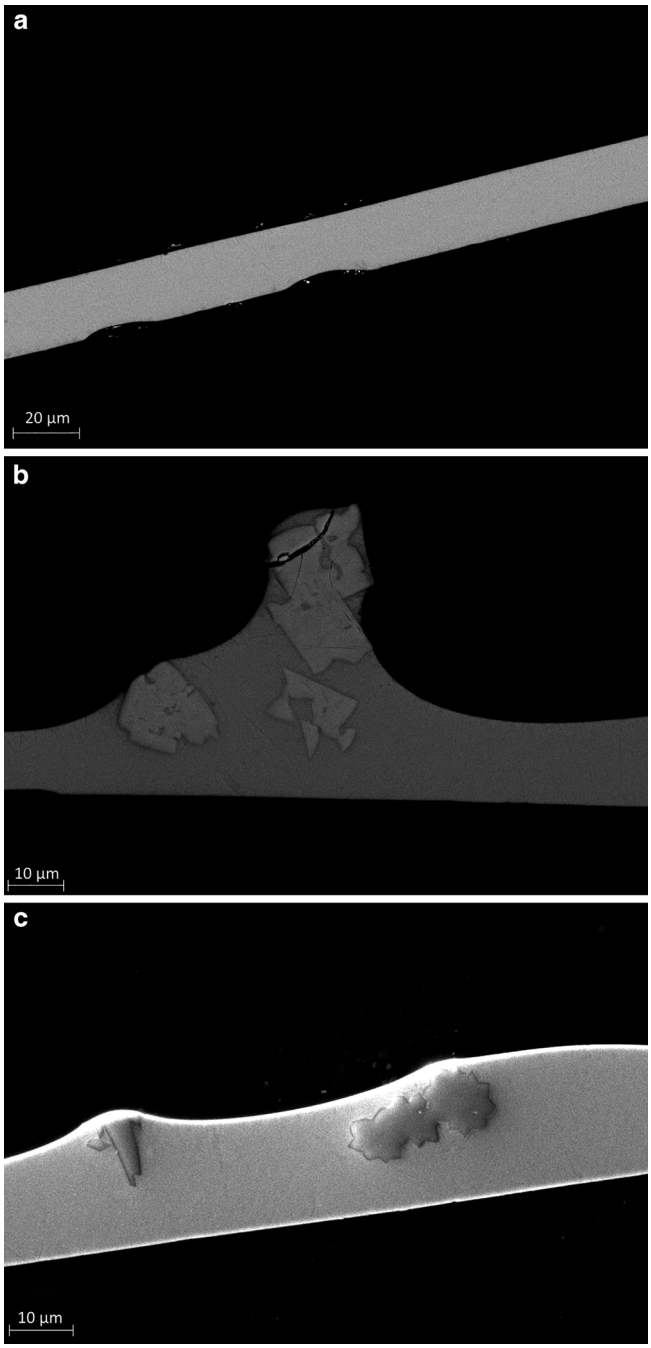

Fig. 2 SEM images of alloys: **a** Mo-20B; **b** Mo,V–20B; **c** V–20B. The air-facing side of the ribbon is closer to the top edge of the image

primary crystallization of the amorphous phase, followed by subsequent high-temperature reactions. It should be noted that an increase in the boron content in the compositions of the Mo,V–B and V–B alloy groups with 17 to 22 at. % boron either mildly affects the crystallization temperature of the alloys (in case of the Mo,V–B group), or lowers it (in case of the V–B group). An increase in the boron content to 25 at. % in these alloys not only causes a change in the nature of the exothermic reaction, but also results in the formation of a supercooled liquid region, from which crystallization begins.

The dependencies of the alloy crystallization temperature on the boron content in the alloy composition are shown in Fig. 4d. In the Mo–V group alloys, the crystallization temperature seemingly increases at higher boron contents. The replacement of molybdenum with vanadium leads to an increase in the crystallization temperatures

Table 2 Results of X-ray microanalysis of the studied alloy ribbons

Alloy	Analysis range	Alloying element content, at. %					
		Fe	Co	Ni	Cr	Mo	V
Mo–20B	Amorphous matrix	25.0 ± 0.4	23.4 ± 0.3	23.6 ± 0.5	13.2 ± 0.3	14.8 ± 0.2	
	Crystal						
Mo,V–20B	Amorphous matrix	25.9 ± 0.5	24.7 ± 0.4	27.5 ± 0.4	11.8 ± 0.2	4.8±0.1	5.3 ± 0.2
	Crystal	11.4 ± 0.2	7.4 ± 0.1	3.6 ± 0.2	22.6 ± 0.5	35 ± 0.5	20 ± 0.5
V–20B	Amorphous matrix	26.5 ± 0.4	22.7 ± 0.3	28.6 ± 0.5	11.9 ± 0.3	–	10.3±0.2
	Crystal	4.4 ± 0.1	2.2 ± 0.1	–	37.4 ± 0.4		56.0 ± 0.6

of alloys containing 17% B, while a further increase in the boron content in the Mo,V–B alloys results in lower crystallization temperatures compared to the Mo–B alloys. At the same time, an increase in the boron content in the Mo,V–B alloys leads to higher crystallization temperatures. Complete replacement of molybdenum with vanadium leads to lower alloy crystallization temperatures when the boron content is increased to 22%. The change in the crystallization process and the appearance of a supercooled liquid region lead to a sharp increase in the crystallization temperature of the Mo,V–25B and V–25B alloys.

The mechanism and temperature of crystallization of the amorphous matrix depend on its composition. The presence of boron in the amorphous phase has a significant impact on the nature of its crystallization [19, 33]. The formation in the ribbon structure of nitride particles, containing a significant amount of dissolved boron, leads to boron depletion of the matrix, which in turn affects the characteristic temperatures and crystallization process of the amorphous matrix.

The replacement of molybdenum with vanadium in the alloys $(Fe_{0.25}Ni_{0.25}Co_{0.25}Cr_{0.125}Mo_{0.125-x}V_x)_{100-y}B_y$, where $x = 0$; 0.0625; 0.125 and $y = 17$–25, leads to the formation of refractory compounds (V,Cr,Mo)(N,B) with an FCC lattice in the alloy structure. Vanadium, molybdenum, and chromium are infinitely soluble in each other, facilitating the easy substitution of one element's atoms with another. These metals possess a strongly negative enthalpy of mixing with nitrogen (–143; –115; and –107 kJ/mol) [34]. Such low enthalpy values lead to the formation of stable insoluble compounds formed by these metals with nitrogen during melting. Furthermore, it is known that zirconium and hafnium nitrides, the crystalline structure of which is similar to that of chromium and vanadium nitrides, can dissolve a significant amount of boron [31]. Therefore, the ribbon structure exhibits the presence of a complex boron-containing compound with an FCC lattice. Boron is a key element that affects the glass-forming ability of amorphous iron-based alloys [17]. The formation of boron-containing crystals in the structure depletes the amorphous matrix of boron, which in turn leads to a decrease in its glass-forming ability and thermal stability. Apparently, an increase in the boron content in the alloy composition suppresses nitride formation during melting. Hence, the structure of high-boron alloys does not contain any crystalline components. Although nitrogen was not intentionally introduced into the alloy, its content in the initial charge material is not regulated by standards. It is known, however, that it can be present in large quantities in the initial charge materials [35, 36]. Additions of chromium, iron, and molybdenum increase the solubility of nitrogen in nickel alloys [37, 38], while nitrogen is also highly soluble in austenitic stainless steels [39]. The addition of vanadium to the alloys leads to the formation of vanadium-based nitrides in the structure. The melting temperature of nitrides is quite high (in excess of 2000 °C), and they are practically insoluble in iron-based alloys. Nitrides formed during the ingot production process do not dissolve when heated for quenching from the liquid state, and are pushed towards the air-facing (upper) surface of the ribbon due to the difference in densities. An increase in the boron content in the alloy composition leads to a shift in the phase equilibrium towards the formation of readily soluble borides in the material structure. Hence, no nitride formation is observed in the structure of vanadium alloys with high boron content, and the replacement of molybdenum with vanadium leads to stabilization of the supercooled liquid upon heating.

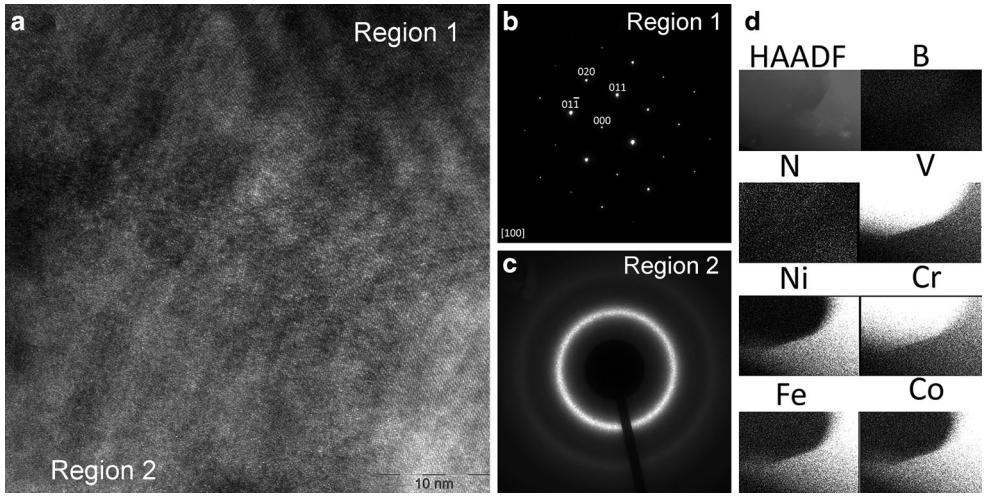

Fig. 3 High-resolution TEM image of the alloy structure (**a**), diffraction patterns from different areas (**b**, **c**), and a chemical element distribution map (**d**)

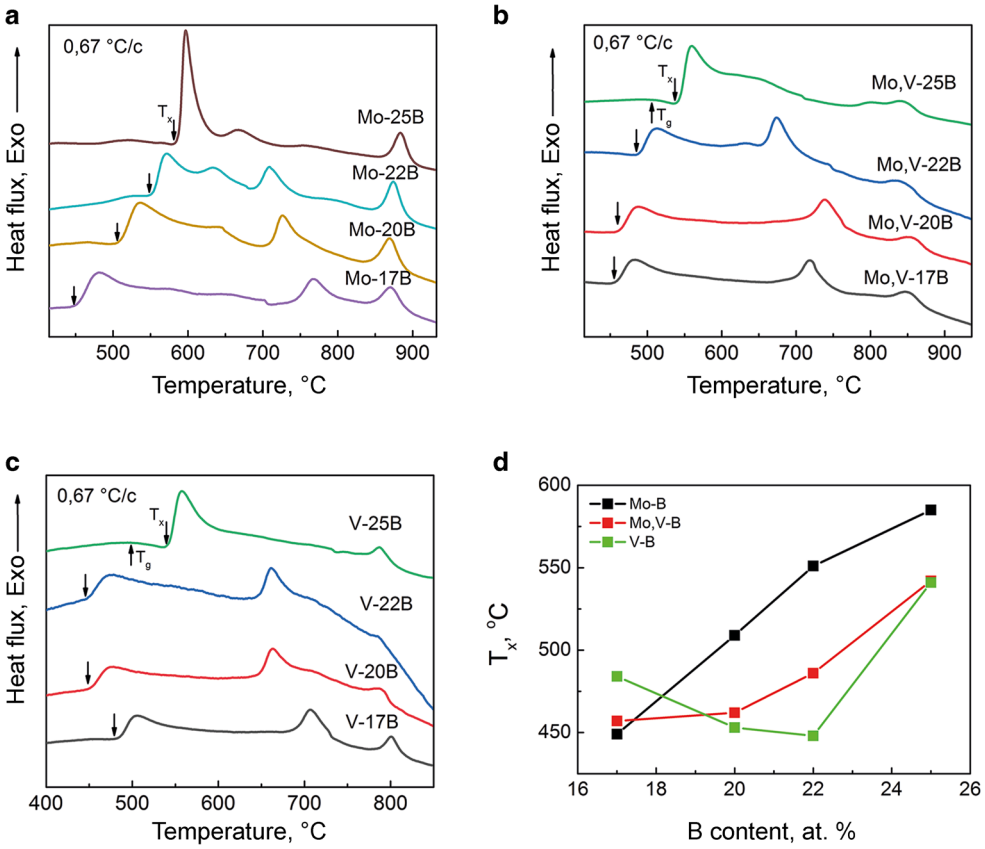

Fig. 4 DSC curves of alloys: **a** Mo-B group; **b** Mo,V–B group; **c** V–B group; **d** alloy crystallization temperatures vs. boron content

According to the results of comparing completely amorphous alloys containing various amounts of vanadium and 25% boron, the presence of vanadium enhances the thermal stability of the supercooled liquid. The endothermic devitrification effect observed on the DSC curves indicates the presence of a temperature range, within which the supercooled liquid exists prior to the onset of alloy crystallization. This range constitutes 37 K and 43 K for the Mo,V–25B and V–25B alloys, respectively. Thus, an increase in vanadium content in the amorphous phase leads to an extension of the existence range of the supercooled liquid, which is indicative of the increased glass-forming ability of the alloys.

Conclusions

The authors analyzed the effect of replacing molybdenum with vanadium in alloys of the $(Fe_{0.25}Ni_{0.25}Co_{0.25}Cr_{0.125}Mo_{0.125-x}V_x)_{100-y}B_y$ system, where $x = 0$; 0.0625; 0.125 and $y = 17–25$. It was found that partial and complete replacement of molybdenum with vanadium leads to the formation of crystalline nitride particles based on V, Cr, and Mo in the structure of low-boron alloy ribbons. It was established that nitrides contain a large amount of dissolved boron, which results in boron depletion of the amorphous matrix and reduction in its thermal stability. In alloys with a completely amorphous structure and high boron concentration, an increase in vanadium content stabilizes the supercooled liquid and expands the temperature range of its existence. The replacement of molybdenum with vanadium in low-boron alloys causes the formation of a partially crystalline structure, consisting of an amorphous matrix and nitride particles. An increase in the boron content to 22–25 at. % leads to thermal stabilization of the amorphous matrix and the appearance of a temperature range of existence of the supercooled liquid.

Acknowledgements The authors express gratitude to the SPbU Interdisciplinary Resource Center for Nanotechnologies for assistance in conducting the SEM and TEM studies.

Funding *The study was sponsored by the Russian Science Foundation, grant No. 22-79-10055,* https://rscf.ru/project/22-79-10055/.

References

1. Cantor B et al (2004) Microstructural development in equiatomic multicomponent alloys. Mater Sci Eng A 375–377(1/2): 213–218
2. Tong C-J et al (2005) Microstructure characterization of Alx CoCrCuFeNi high-entropy alloy system with multiprincipal elements. Met Mater Trans A 36(4):881–893
3. Zuo TT et al (2014) Effects of Al and Si addition on the structure and properties of CoFeNi equal atomic ratio alloy. J Magn Magn Mater 371:60–68
4. Zhang Y et al (2014) Microstructures and properties of high-entropy alloys. Prog Mater Sci 61:1–93
5. Miracle DB, Senkov ON (2017) A critical review of high entropy alloys and related concepts. Acta Mater 122:448–511
6. Senkov ON et al (2011) Mechanical properties of $Nb_{25}Mo_{25}Ta_{25}W_{25}$ and $V_{20}Nb_{20}Mo_{20}Ta_{20}W_{20}$ refractory high entropy alloys. Intermetallics 19(5):698–706
7. Zhang Y, Yang X, Liaw PK (2012) Alloy design and properties optimization of high-entropy alloys. JOM 64(7):830–838
8. Zhang Y et al (2008) Solid-Solution phase formation rules for multi-component alloys. Adv Eng Mater 10(6):534–538
9. Guo S, Liu CT (2011) Phase stability in high entropy alloys: formation of solid-solution phase or amorphous phase. Prog Nat Sci Mater 21(6):433–446
10. Ding HY et al (2014) A senary TiZrHfCuNiBe high entropy bulk metallic glass with large glass-forming ability. Mater Lett 125:151–153
11. Zhao K et al (2012) Formation and properties of strontium-based bulk metallic glasses with ultralow glass transition temperature. J Mater Res 27(20):2593–2600
12. Takeuchi A et al (2011) $Pd_{20}Pt_{20}Cu_{20}Ni_{20}P_{20}$ high-entropy alloy as a bulk metallic glass in the centimeter. Intermetallics 19(10):1546–1554
13. Molotilov BV et al (2006) Development and production of amorphous and nanocrystalline materials. Metallurgist 50(3/4):209–212
14. Inoue A (2000) Stabilization of metallic supercooled liquid and bulk amorphous alloys. Acta Mater 48(1):279–306
15. Li Y, Zhang W, Qi T (2017) New soft magnetic $Fe_{25}Co_{25}Ni_{25}(P, C, B)_{25}$ high entropy bulk metallic glasses with large supercooled liquid region. J Alloys Compd 693:25–31
16. Qi T et al (2015) Soft magnetic $Fe_{25}Co_{25}Ni_{25}(B, Si)_{25}$ high entropy bulk metallic glasses. Intermetallics 66:8–12
17. Ding J et al (2017) High entropy effect on structure and properties of (Fe,Co,Ni,Cr)-B amorphous alloys. J Alloys Compd 696:345–352
18. Gerasimov MV, Simirskii YN (2008) Relationship between the electrochemical behavior of phosphides and amorphous iron alloys that contain chromium and phosphorus. Metallurgist 52(7/8):477–481
19. Wang F et al (2018) Formation, thermal stability and mechanical properties of high entropy (Fe,Co,Ni,Cr,Mo)-B amorphous alloys. J Alloys Compd 732:637–645
20. Wang F et al (2019) Formation, stability and ultrahigh strength of novel nanostructured alloys by partial crystallization of high-entropy $(Fe_{0.25}Co_{0.25}Ni_{0.25}Cr_{0.125}Mo_{0.125})_{86-89}B_{11-14}$ amorphous phase. Acta Mater 170:50–61

21. Wang F et al (2017) Soft magnetic Fe-Co-based amorphous alloys with extremely high saturation magnetization exceeding 1.9 T and low coercivity of 2 A/m. J Alloys Compd 723:376–384
22. Liu Ch-Ts et al (2020) Microstructures and mechanical properties of CoCrFeMnNiVx high entropy alloy films. J Alloys Compd 820:1–8
23. Lv K et al (2022) Enhanced glass forming ability and excellent saturation magnetic flux density by V addition in FeSiBPCCu amorphous/noncrystalline alloys. Intermetallics 148:107623
24. Chen L et al (2023) Exploration of V–Cr–Fe–Co–Ni high-entropy alloys with high yield strength: A combination of machine learning and molecular dynamics simulation. Comput Mater Sci 217:111888
25. Reed RP (1989) Nitrogen in austenitic stainless steels. JOM 41(3):16–21
26. Hertzman S et al (2021) Nitrogen solubility in alloy systems relevant to stainless steels. Met Mater Trans A 52(9):3811–3820
27. Sun H, Wang Y (2018) Glass forming ability, thermal stability, and magnetic properties of FeCoNiBSi alloys with different B contents. Adv Mater Sci Eng 2018:1–6
28. Venkatraman M, Neumann JP (1987) The cr–Mo (chromium–molybdenum) system. Bull Alloy -ph Diagrams 8(3):216–220
29. Predel F (2016) Phase diagram of Mo–V (molybdenum–vanadium) system. In: Predel F (ed) Phase equilibria, crystallographic and thermodynamic data of binary alloys. Springer, Berlin, Heidelberg
30. Smith JF, Bailey DM, Carlson ON (1982) The Cr-V (Chromium-Vanadium) system. J Phase Equilibria 2(4):469–473
31. Rudy E, Benesovsky F (1961) Untersuchungen in den systemen: hafnium-Bor-Stickstof und Zirkonium-Bor-Stickstoff. Monatsh Chem 92(2):415–441
32. Spear K, Schäfer H, Gilles P (1968) The vanadium-boron-nitrogen system. J Less Common Met 14(4):449–457
33. Wang A et al (2016) Composition design of high B s Fe-based amorphous alloys with good amorphous-forming ability. J Alloys Compd 656:729–734
34. Takeuchi A, Inoue A (2005) Classification of bulk metallic glasses by atomic size difference, heat of mixing and period of constituent elements and its application to characterization of the main alloying element. Mater Trans 46(12):2817–2829
35. Mills T (1971) The solubility of nitrogen in solid chromium. J Less Common Met 23(4):317–324
36. Abdulrahman RF, Hendry A (2001) The solubility of nitrogen in liquid pure nickel. Met Mater Trans B 32(6):1095–1101
37. Kowanda C, Speidel M (2003) Solubility of nitrogen in liquid nickel and binary Ni-Xi alloys (Xi=Cr, Mo, W, Mn, Fe, Co) under elevated pressure. Scr Mater 48(8):1073–1078
38. Abdulrahman RF, Hendry A (2001) Solubility of nitrogen in liquid nickel-based alloys. Met Mater Trans B 32(6):1103–1112
39. Kobayashi Y et al (2012) Solubility of nitrogen in Fe-Cr-Ni-Mo stainless steel under a 1 atm N_2 gas atmosphere. Isij Intern 52(9):1601–1606

Authors and Affiliations

✉ A. I. Bazlov
bazlov@misis.ru

I. V. Strochko
istrochko@icloud.com

E. N. Zanaeva
zanaeva@misis.ru

E. V. Ubyivovk
ubyivovk@gmail.com

M. S. Parkhomenko
parkhomenko.m@misis.ru

D. A. Milkova
milkovadaria@gmail.com

V. V. Briukhanova
verabryu@gmail.com

A. I. Bazlov, I. V. Strochko, E. V. Ubyivovk, D. A. Milkova, V. V. Briukhanova
Saint Petersburg State University, St. Petersburg, Russian Federation

A. I. Bazlov, E. N. Zanaeva, M. S. Parkhomenko, D. A. Milkova
National University of Science and Technology “MISIS”, Moscow, Russian Federation